Supplemental Data, Streb et al. (2008). Starch granule biosynthesis in Arabidopsis is abolished by removal of all debranching enzymes, but restored by the subsequent removal of an endoamylase.

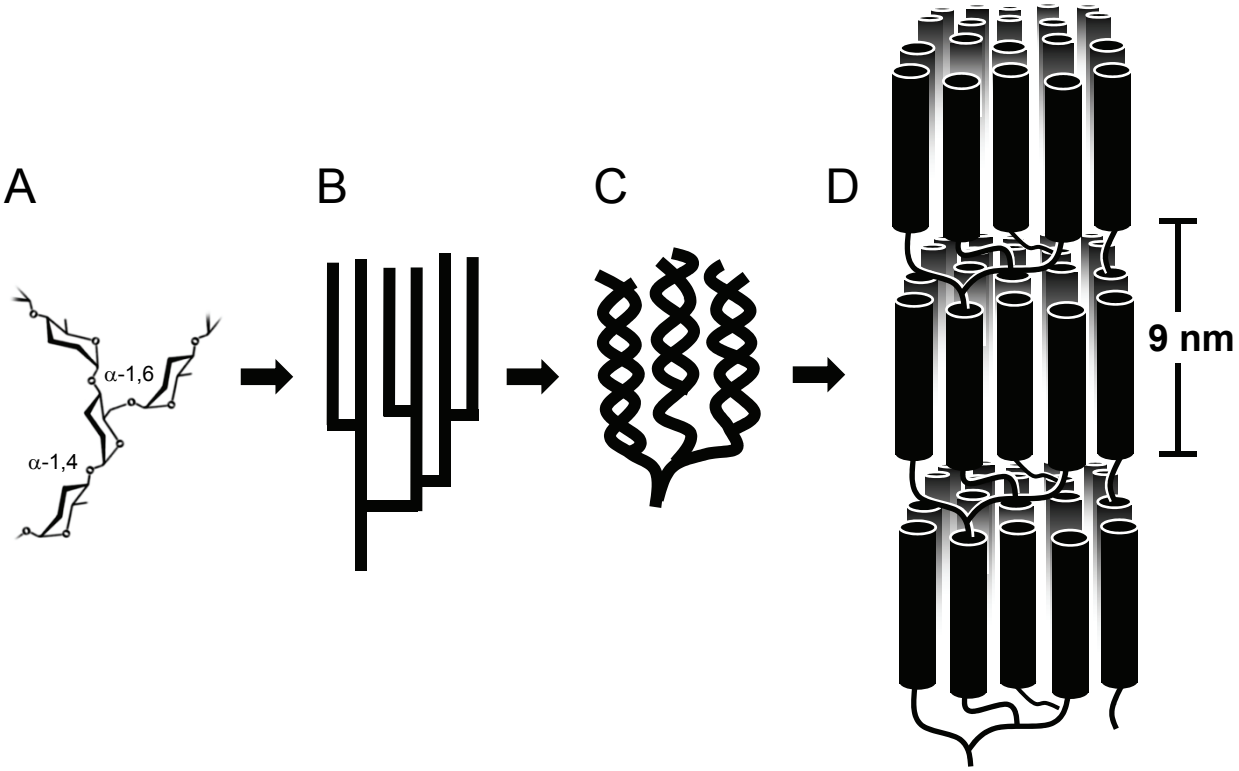

Supplemental Figure 1. A model of amylopectin structure.

A. Glucose molecules are linked via α-1,4-bonds to form chains that are connected via α-1,6-branch points.

B. Branch points are arranged in such a way as to generate clusters of adjacent, unbranched chains. The precise architecture of amylopectin is not known.

C. Neighbouring chains of sufficient length (≥ d.p. 12) interact to form double helices.

D. Double helices (here depicted as cylinders) pack to form regular, semi-crystalline lamellae which alternate with amorphous lamellae where the branch points are located. The periodicity of this repeated structure is 9 nm.

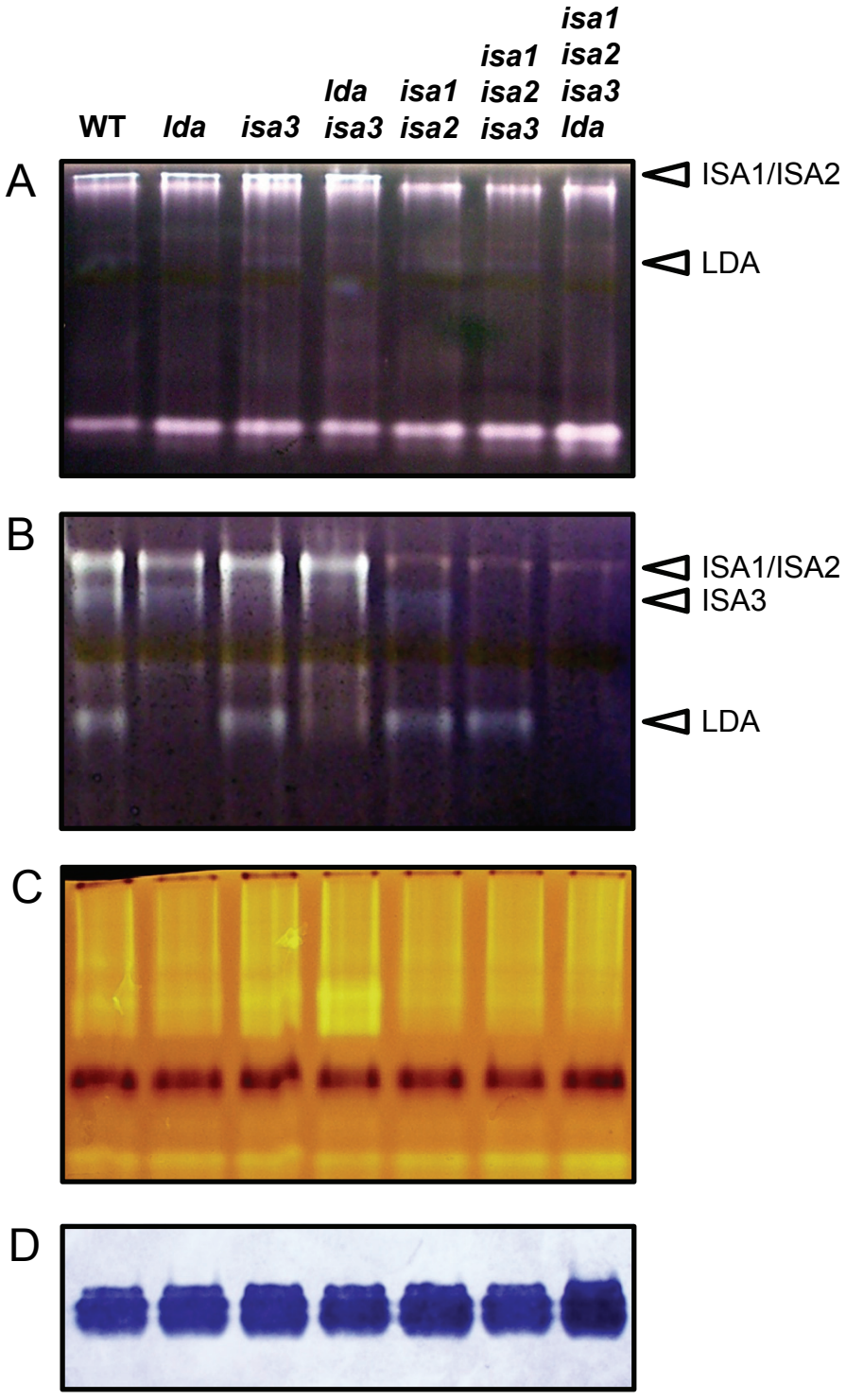
WT
lda
isa3
lda isa3
isa1 isa2
isa1 isa2 isa3
isa1 isa2 isa3 lda
A
ISA1/ISA2
LDA
B
ISA1/ISA2
ISA3
LDA
C
D

Supplemental Figure 2. Analysis of glucan metabolising enzymes using native PAGE.

Proteins extracted from leaves of the wild type (WT) and the DBE mutant combinations (as indicated) were separated by native PAGE.

A. Detection of starch hydrolysing enzymes in gels containing amylopectin. After electrophoresis, the gels were incubated for 2 h and then stained with iodine solution to reveal pale bands where the amylopectin had been hydrolysed. The ISA1/ISA2 isoamylase activity is visible as the uppermost band, and LDA activity as a faint blue band. ISA3 activity is not visible.

B. Detection of starch hydrolysing enzymes in gels containing β-limit amylopectin. After electrophoresis, the gels were incubated for 2 h and then stained with iodine solution to reveal pale bands where the β-limit amylopectin had been hydrolysed. All three debranching enzyme activities are visible.

C. Detection of starch synthase isoforms in glycogen containing gels. After electrophoresis, the gels were incubated for 2 h in medium containing 2 mM ADPGlc and then stained with iodine solution to reveal dark bands where starch synthase had elongated linear chains. Pale band where hydrolytic enzymes have degraded the glycogen are also visible.

D. Detection of branching enzyme isoforms in glycogen containing gels. After electrophoresis, the gels were incubated for 2 h in medium containing 50 mM Glc 1-P and 50 units of rabbit muscle phosphorylase *a*, then stained with iodine solution to reveal dark bands where the combination of phosphorylase and branching enzyme have synthesised glucans. Activity in the quadruple DBE mutant was slightly elevated. Replicate gels established that this increase was less than two-fold (not shown).

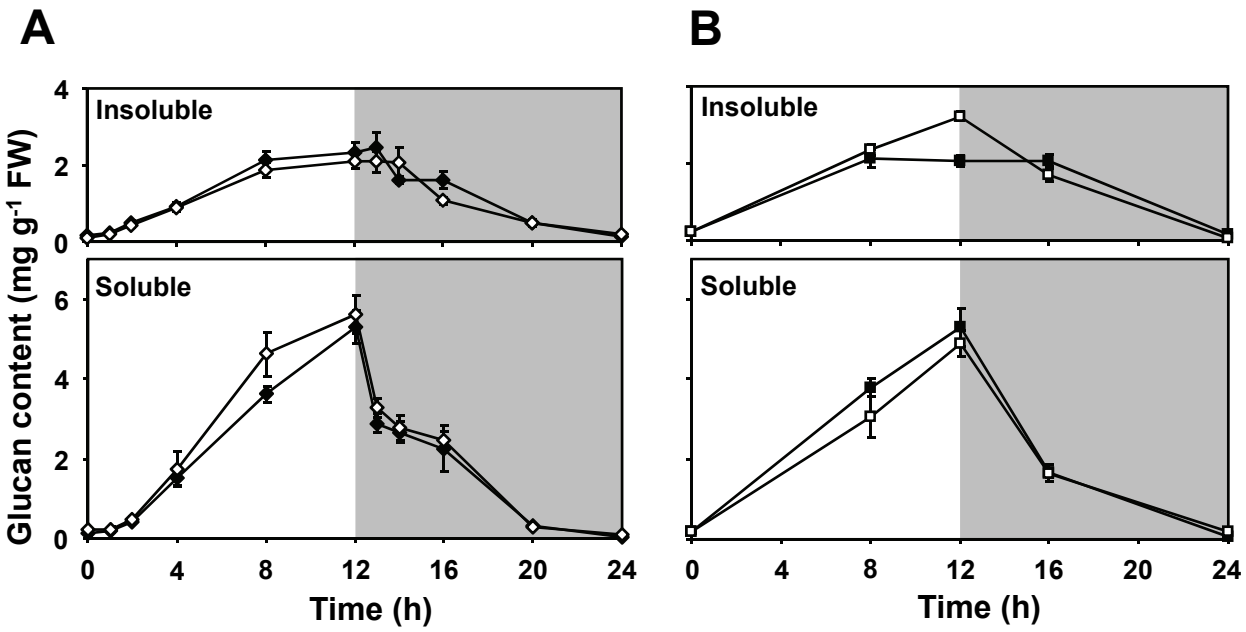

Supplemental Figure 3. Comparison of the glucan contents of *isa1*/*lda* and *isa2*/*lda* double mutants with the respective *isa* single mutants.

Samples were harvested, extracted and measured as in Figure 1. Each point is the mean ± standard error from five replicate samples. Wild-type and *lda* plants grown in parallel had, respectively, 12.5 ± 0.7 and 11.8 ± 0.4 mg starch g^{-1} fresh weight at the end of the day.

A. Insoluble and soluble glucan content of *isa1* plants (black circles) and *isa1*/*lda* plants (white circles).

B. Insoluble and soluble glucan content of *isa2* plants (black squares) and *isa2*/*lda* plants (white squares). Only at one time point (end of the day) was a difference measured between *isa2*/*lda* and *isa2*. The double mutant had more starch than the single mutant – the reverse of the observation reported by Wattebled et al. (2005). However, given the overall similarity between the lines and the results in Figure 1A, it seems likely that the difference between *isa2*/*lda* and *isa2* at this single time point is due to biological variation.

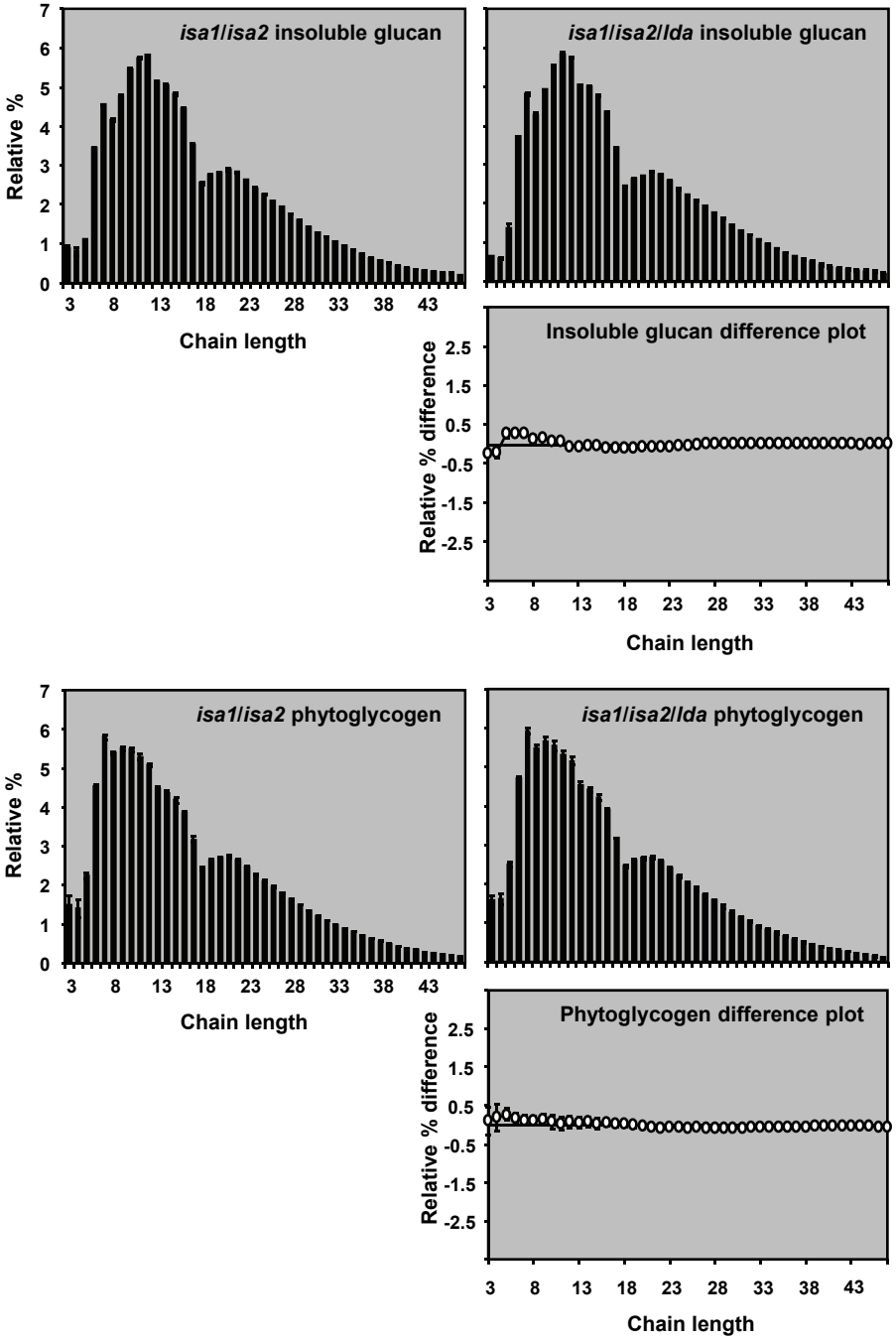

Supplemental Figure 4. Comparisons of the chain length distributions of glucans extracted from leaves of the *isa1*/*isa2* double mutant and the *isa1*/*isa2*/*lda* triple mutant.

Glucans extracted from plants harvested at the end of the day were analysed as in Figure 2. The means ± standard errors of three technical replicate digests are shown. Difference plots were derived by subtracting the relative percentage values of the *isa1*/*isa2* from those of *isa1*/*isa2*/*lda*. The standard errors of the compared data sets were added together.

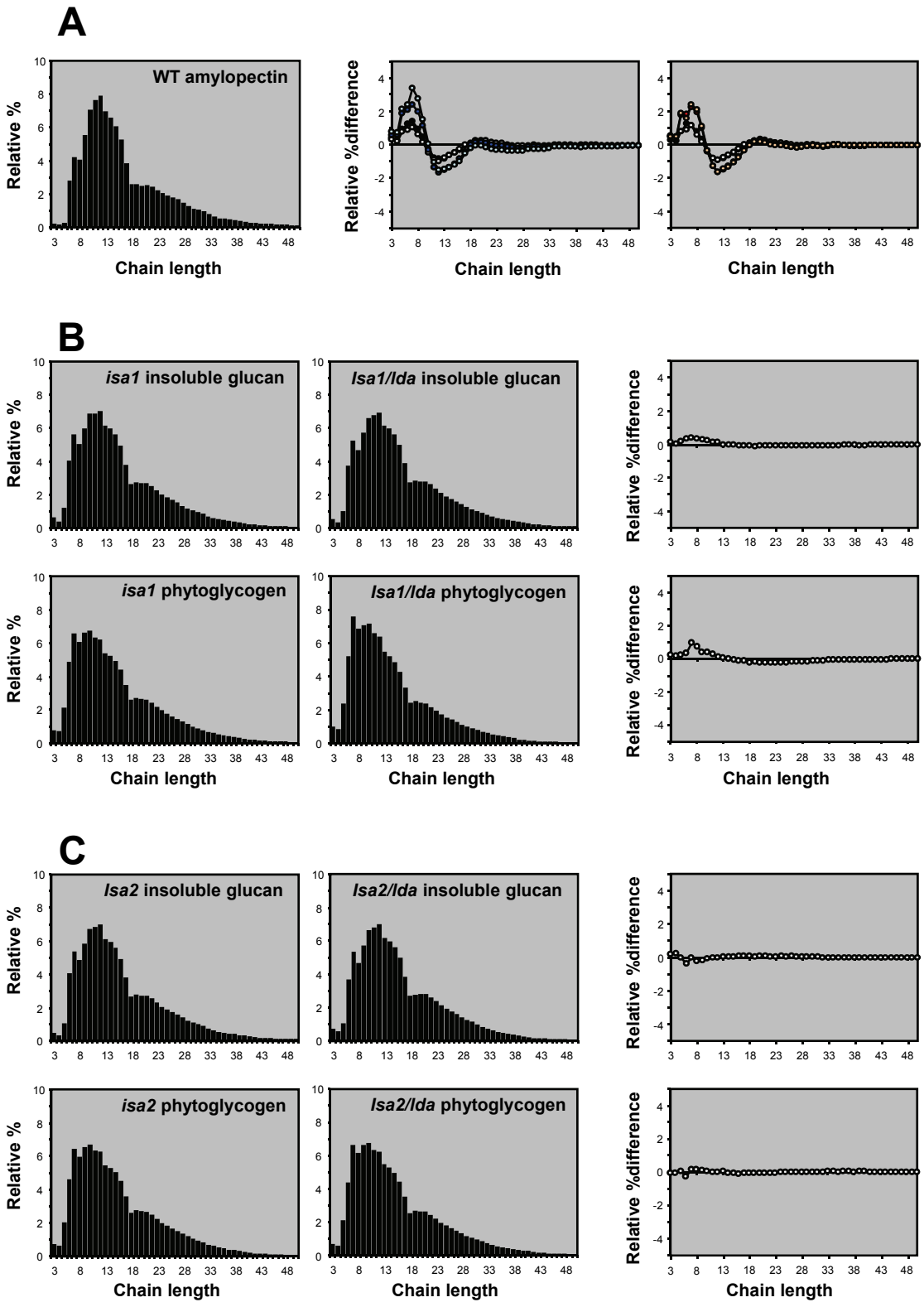
A
WT amylopectin
Relative %
Relative %difference
Chain length
B
isa1 insoluble glucan
Isa1/lda insoluble glucan
isa1 phytoglycogen
Isa1/lda phytoglycogen
C
Isa2 insoluble glucan
Isa2/lda insoluble glucan
isa2 phytoglycogen
Isa2/lda phytoglycogen

Supplemental Figure 5. Comparisons of the chain length distributions of glucans extracted from leaves of the *isa1*and *isa2* single mutants, and the *isa1*/*lda* and *isa2*/*lda* double mutants.

Glucans extracted from plants harvested at the end of the day (Supplemental Figure 3 online) were analysed as in Figure 2. The means of two technical replicate digests are shown.

A. The chain length distribution of wild-type (WT) amylopectin. Difference plots were derived by subtracting the relative percentage values of WT amylopectin from the DBE mutant glucans. Left panel; black circles, *isa1* insoluble glucan; white circles, *isa1*/*lda* insoluble glucan; dark blue circles, *isa1* phytoglycogen; light blue circles, *isa1*/*lda* phytoglycogen. Right panel; black circles, *isa2* insoluble glucan; white circles, *isa2*/*lda* insoluble glucan; red circles, *isa2* phytoglycogen; gold circles, *isa2*/*lda* phytoglycogen.

B. The chain length distribution of *isa1* and *isa1*/*lda* glucans, as indicated. Difference plots were derived by subtracting the relative percentage values of *isa1* from the respective *isa1*/*lda* values.

C. The chain length distribution of *isa2* and *isa2*/*lda* glucans, as indicated. Difference plots were derived by subtracting the relative percentage values of *isa2* from the respective *isa2*/*lda* values.

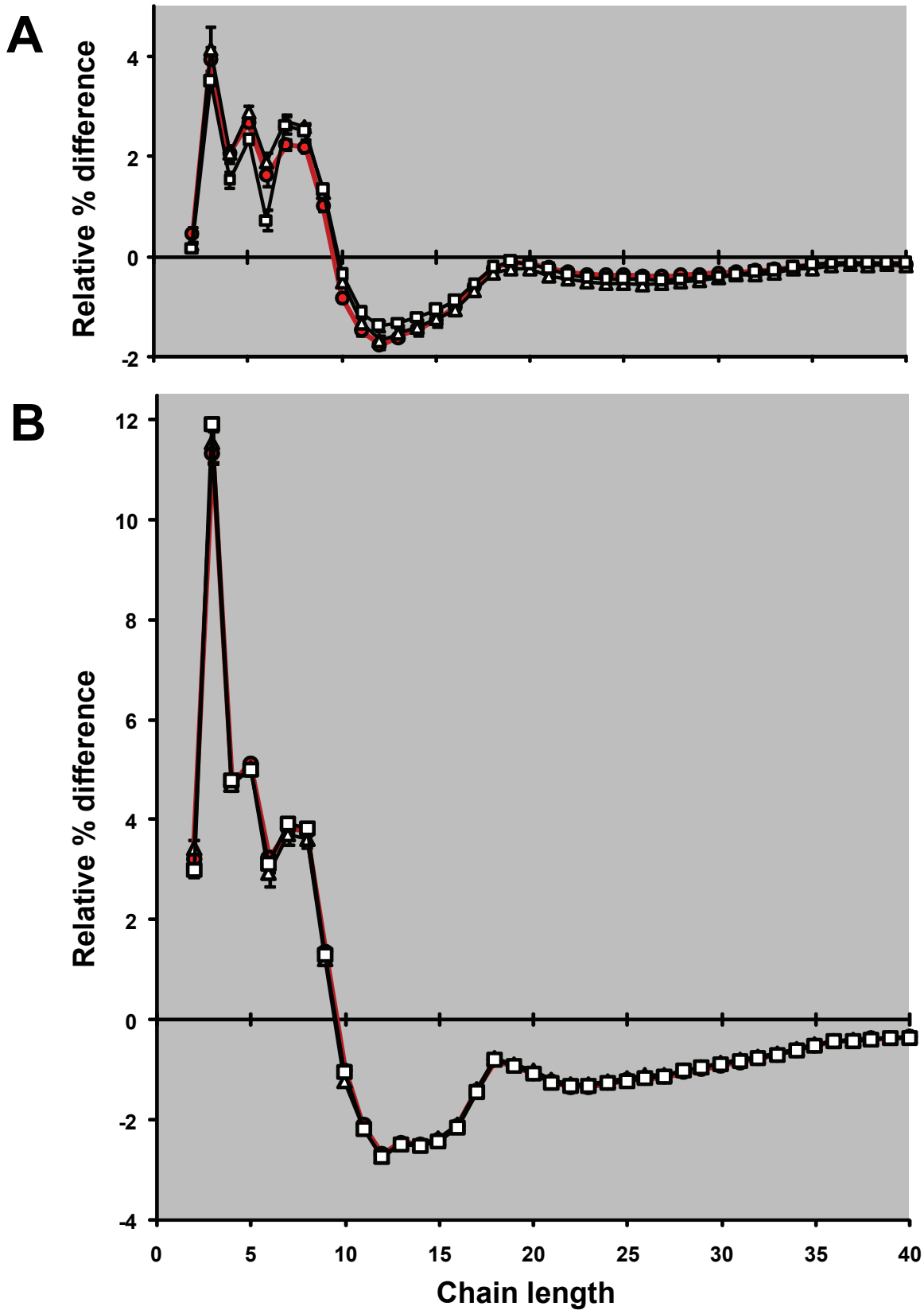
A
Relative % difference
4
2
0
-2
B
Relative % difference
12
10
8
6
4
2
0
-2
-4
0
5
10
15
20
25
30
35
40
Chain length

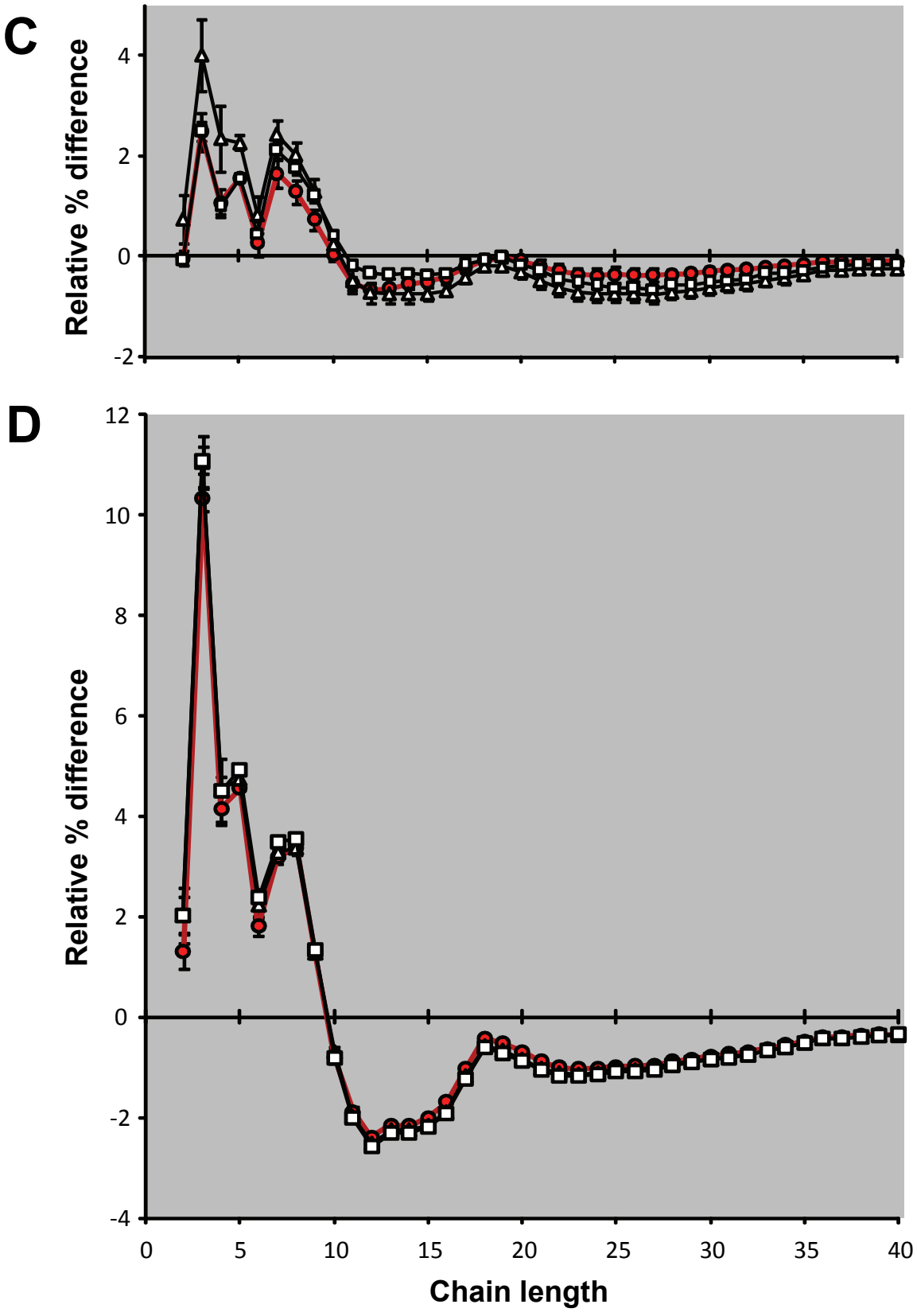
C
Relative % difference
4
2
0
-2
D
Relative % difference
12
10
8
6
4
2
0
-2
-4
0
5
10
15
20
25
30
35
40
Chain length

Supplemental Figure 6. Equivalence between the chain length distributions of the glucans within the mutant groups *isa1*/*isa3*, *isa2*/*isa3, isa1*/*isa2*/*isa3* and *isa1*/*isa3*/*lda*, *isa2*/*isa3*/*lda, isa1*/*isa2*/*isa3*/*lda*.

Glucans extracted from plants harvested at the end of the day were analysed in triplicate as in Figure 2. The standard errors of the compared data sets were added together.

A. The difference plots for the soluble glucans of *isa1*/*isa3* (white squares), *isa2*/*isa3* (white triangles) and *isa1*/*isa2*/*isa3* (red circles – data as in Figure 2) were derived by subtracting the relative percentage values of wild-type amylopectin.

B. Difference plots for the soluble glucans of *isa1*/*isa3*/*lda* (white squares), *isa2*/*isa3*/*lda* (white triangles) and *isa1*/*isa2*/*isa3*/*lda* (red circles – data as in Figure 2) were derived by subtracting the relative percentage values of wild-type amylopectin.

C. The difference plots for the insoluble glucans of *isa1*/*isa3* (white squares), *isa2*/*isa3* (white triangles) and *isa1*/*isa2*/*isa3* (red circles – data as in Figure 2) were derived by subtracting the relative percentage values of wild-type amylopectin.

D. Difference plots for the insoluble glucans of *isa1*/*isa3*/*lda* (white squares), *isa2*/*isa3*/*lda* (white triangles) and *isa1*/*isa2*/*isa3*/*lda* (red circles – data as in Figure 2) were derived by subtracting the relative percentage values of wild-type amylopectin.

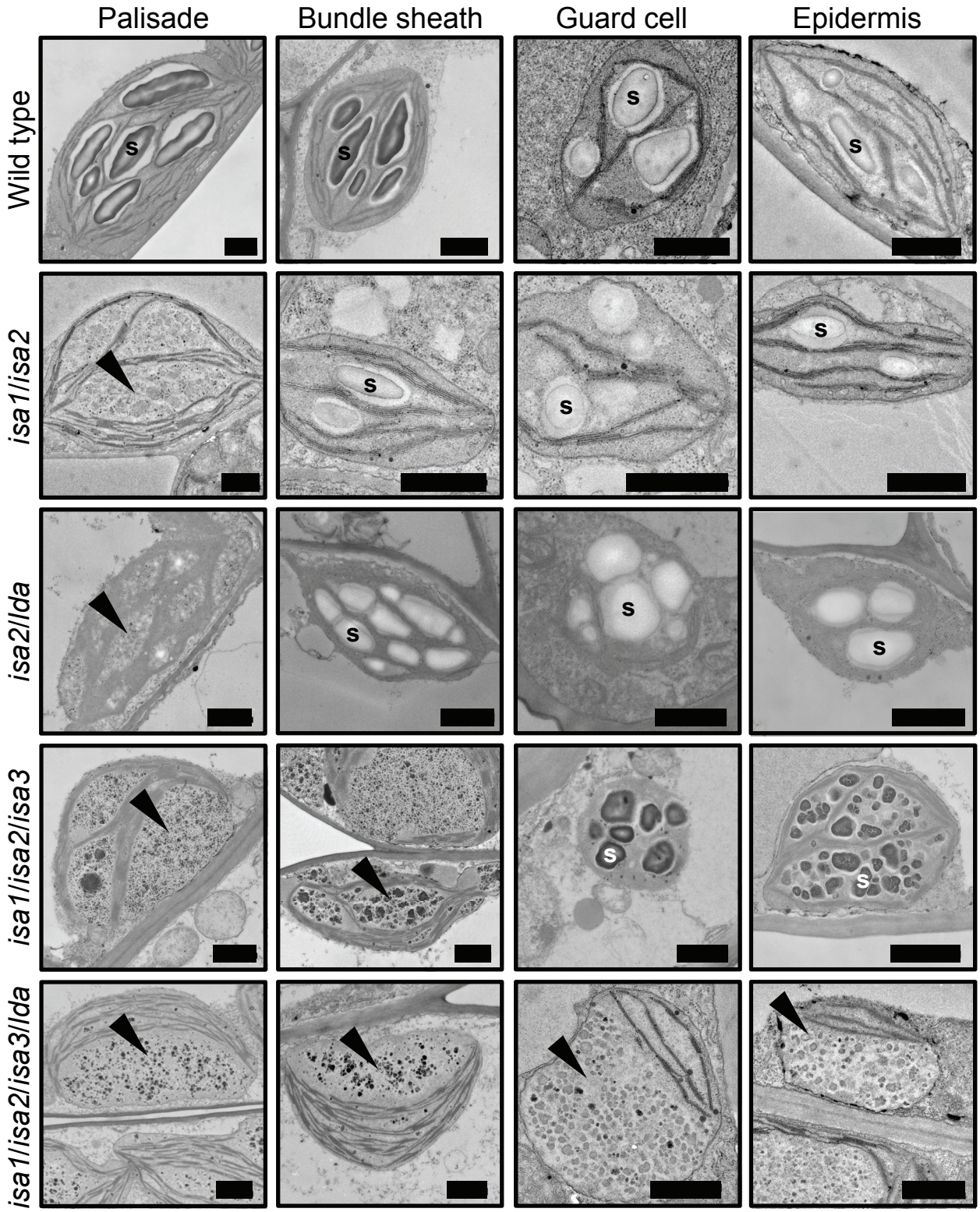
Palisade
Bundle sheath
Guard cell
Epidermis
Wild type
isa1/isa2
isa2/lda
isa1/isa2/isa3
isa1/isa2/isa3/lda
S

Supplemental Figure 7. Visualisation of the glucans accumulating in plastids of different cell types of wild-type and DBE mutant plants using transmission electron microscopy.

Cell types and mutant combinations are as given above and to the left, respectively. Bars = 1 μm. Starch granules (s) and soluble or particulate material (arrows) are indicated. Differences in the darkness of the starch granules (e.g. in the wild-type sections) reflects variation in staining intensity between sections and did not correlate with genotype.

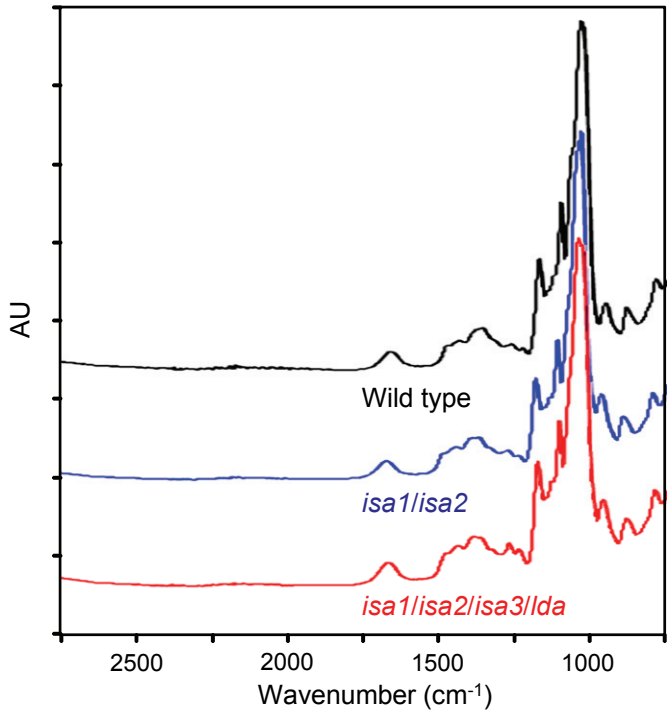

Supplemental Figure 8. FTIR spectra of wild-type starch and the insoluble glucans from *isa1*/*isa2*, and the quadruple DBE mutant.

The peaks around wavenumber 1000 cm^{-1} are typical of starch. Proteins give rise to peaks at approximately 1500 and 1700 cm^{-1}. AU, arbitrary units.

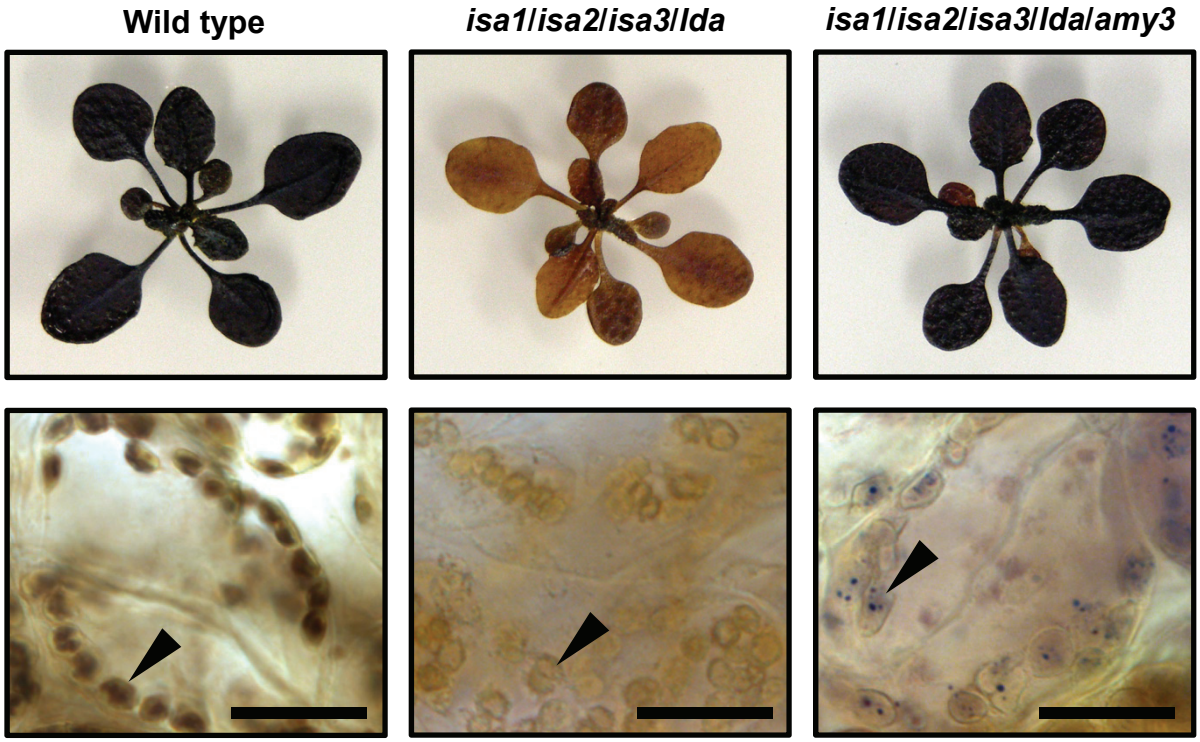

Supplemental Figure 9. Iodine staining of wild-type, *isa1*/*isa2*/*isa3*/*lda* quadruple mutant and *isa1*/*isa2*/*isa3*/*lda*/*amy3* quintuple mutant plants.

Plants were harvested at the end of a 12-h photoperiod, decolourised with hot ethanol and stained for starch with iodine solution. Top row, whole rosettes; bottom row, mesophyll cells viewed by light microscopy. Arrows indicate individual chloroplasts. Note the dark-staining particles in the quintuple mutant. Bars = 20 µm.

Supplemental Table 1. Debranching enzyme genes and the respective mutant lines. Those used in this study are given in bold.

Gene AGI code	Gene length (ORF) / exons	Mutation type, position	Mutant alleles (other nomenclature)	Line identifier	Genotyping primers used in this study (shown 5' to 3')	Ecotype*	References
ISA1 At2g39930	6105bp / 18	**T-DNA insertion, exon13**	***Atisa1*-1**	**SALK_042704**	Fwd: GGGACAGCCTATGTGATCTGCC Rev: TGGGAAACCATGAGGGAAACA T-DNA: GCGTGGACCGCTTGCTGCAACT	**Col-0**	Delatte et al. (2005) Wattebled et al. (2005)
ISA2 At1g03310	2648bp / 1	**Single base-pair deletion, exon 1**	***Atisa2*-1 (*dbe1*-1)**	-	Fwd: GGTGACGTATTTACCGATGGA Rev: TGACACTTTGAGCAGCAACC The *Atisa2*-1 amplicon is cut by NlaIV	**Col-0**	Zeeman et al. (1998a) Delatte et al. (2005)
		T-DNA insertion, exon 1	*Atisa2*-2	SALK_029442		Col-0	Wattebled et al. (2005)
		Promoter or 5'UTR	*Atisa2*-3** *(Atisa2*-1*)*	Génoplante_CTI15		WS	Wattebled et al. (2005)
		Unknown	*Atisa2*-4 (*dbe1*-2)			Col-0	Zeeman et al. (1998a)
ISA3 At4g09020	4740bp / 24	T-DNA insertion, intron 18	*Atisa3*-1	SALK_104008		Col-0	Wattebled et al. (2005)
		T-DNA insertion, exon 21	***Atisa3*-2**	**GABI_280G10**	Fwd: GATCTTCCGATCTTTACCAGGTTA Rev1: ACTGGAGAAGGATTGAAGAGAATG Rev2: CTTACTTGGACTGGAGAAGGATTG T-DNA: CCCATTTGGACGTGAATGTAGACA	**Col-0**	Delatte et al. (2006)
		G to A substitution, intron 5 to exon 6 splice junction	*Atisa3*-3	CS88929		Col-0	Delatte et al. (2006)
		G to A substitution, exon 14, results in a stop codon	*Atisa3*-4	Deg263		Col-0	Messerli et al. (2007)
LDA At5g04360	6833 / 28	T-DNA insertion, exon 5	*Atlda*-1 (*Atpu1*-1)	Génoplante_CQU5		WS	Wattebled et al. (2005)
		T-DNA insertion, exon 7	***Atlda*-2**	**SALK_060765**	Fwd: TTGCCAACACTAAGAAACTTACGGA Rev: TGTGATTCAAAGATTGACCAAACAA T-DNA: GCGTGGACCGCTTGCTGCAACT	**Col-0**	Delatte et al. (2006)
		T-DNA insertion, exon 12	*Atlda*-3	CSHL_ GT7150		L.*er*	Delatte et al. (2006)

***Wassilewskija (WS), Columbia-0 (Col-0), Landsberg *erecta* (L.*er*); ****Re-named from Wattebled et al. (2005) to avoid confusion with allele published previously in Delatte et al.(2005)